

# Nucleon Properties in the Quantized Linear Sigma Model at Finite Temperature and Chemical Potential

H. M. Mansour<sup>1</sup> and M. Abu-Shady<sup>2</sup>

<sup>1</sup>*Department of Physics, Faculty of Science, Cairo University, Egypt*

<sup>2</sup>*Department of Applied Mathematics,  
Faculty of Science, Menoufia University, Egypt*

(Dated: July 28, 2015)

## Abstract

The linear sigma model at finite temperature and chemical potential is systematically studied using the coherent-pair approximation, in which fully taking quantum of fields are included. The expectation value of the chiral Hamiltonian density is minimized and the resulting equations for the nucleon are solved. The qualitative features of the quantized sigma and pion fields are strong sensitive to the change of temperature and chemical potential and are in agreement with the mean-field approximation calculations. It is noticed that the nucleon mass increases with increasing coherence parameter  $x$ . In addition, the nucleon mass increases with increasing temperature  $T$  and the baryonic chemical potential  $\mu$  and then it decreases at higher values of the temperature and baryonic chemical potential. The obtained results show that the mean-square radius of the proton and the neutron increase with increasing temperature or the baryonic chemical potential and that the pion-nucleon coupling constant  $g_{\pi NN}$  decreases with the temperature or baryonic chemical potential. We conclude that the coherent-pair approximation successfully give better description of the nucleon properties at finite temperature and baryonic chemical potential.

PACS numbers: 11.30 Rd, 12.38Mh, 12.38 Aw, 11.30 QC

Keywords: Effective mesonic potential, chemical potential, finite temperature, nucleon properties

## I. INTRODUCTION

The topic of hot and dense medium is of great interest in the high energy heavy ion collisions [1, 2]. The properties of vacuum at zero temperature and density have different behavior at finite temperature and density due to the chiral symmetry restoration and deconfinement of the system. This gives more insight into the complex vacuum structure of quantum chromodynamic (QCD) theory which describes relevant features of particle physics in the early universe and the neutron stars.

Such investigation unfortunately cannot be calculated directly in the framework of QCD theory. The difficulties involved in obtaining low-energy properties directly from QCD, the fundamental theory of strong interactions is due to its coupling constant at low energy scale and thereby the necessity of dealing non-perturbatively with its complicated structure [3]. Hence, the investigations are usually performed by using the effective models which share the same properties with QCD theory such as the Nambu-Jona-Lasinio (NJL) model [4] and the linear sigma model and its modifications [5 – 11].

At finite temperature and density, the linear sigma model and its modifications show a significant success in the description of chiral phase transition and the static properties of the nucleon such as discussed in Refs. [12 – 19]. There are some limited research works on the nucleon properties at finite temperature and density in the framework of the linear sigma model. Christov et al. [12] studied the modification of baryon properties at finite temperature and density. They ignored quantum fluctuations in their calculations. Dominguez et al. [13] calculated the pion-nucleon coupling constant and the mean square radius of the proton as functions of the temperature. Thermal fluctuations are only considered and they ignored quantum fluctuations in their model. In Ref.[14], the nucleon properties are also studied in the framework of the linear sigma model at finite temperature without including chemical potential in their calculations.

On the other hand, in Refs. [15 – 17], the authors focus on the study of the phase transition and critical point at finite temperature and chemical potential in the framework of the linear sigma model. Bilic and Nikolic [15] studied the chiral transition in the linear sigma model at finite temperature and chemical potential in mean-field approximation. Phat and Thu [18] studied the chiral phase transition and its order at finite temperature and isospin chemical potential using the linear sigma model. Schaefer et al. [19] have extended the quark

sigma model to include certain aspects of the gluon dynamics via the Polyakov loop at finite temperature and quark chemical potential. Mao et al. [20] studied the deconfinement phase transition using the Friedberg-Lee model at finite temperature and chemical potential, and then they obtained the critical value of the temperature and chemical potential. In the NJL model [21], the meson and nucleon properties are studied. they considered the case of a quark medium as well as nucleon medium. They studied the behavior of the nucleon mass and energy of the soliton at different temperatures and densities in the mean-field approximation. Cheng-Fu et al. [22] studied some nucleon properties such as a binding energy using the simplified version of Faddeev equations at finite temperature and chemical potential.

In the present work, we apply the coherent-pair approximation (CPA) in the chiral quark-sigma model at finite temperature and chemical potential. CPA is a powerful nonperturbative method to go beyond the mean-field approximation by fully taking thermal and quantum fluctuations into account [14]. While CPA has already been applied in the chiral quark sigma model at finite temperature only in Ref. [14], so far no attempt has been made to include the finite chemical potential. We continue further study of the investigation that started in Ref. [14]. Here, our aim is to study how the nucleon properties respond when the chemical potential is included in the framework of the linear sigma model using CPA.

In Sec. 2, the effective mesonic potential at finite temperature and the chemical potential is explained. The variational principle is presented in Sec. 3. The derived nucleon properties are calculated at finite temperature and chemical potential in Sec. 4. The numerical calculations and the results are presented in Sec. 5. A summary and conclusions are introduced in Sec. 6.

## II. THE QUARK SIGMA MODEL AT FINITE TEMPERATURE AND CHEMICAL POTENTIAL

The effective mesonic potential describes the interactions of quarks via  $\sigma$  and  $\pi$ -meson at finite temperature  $T$  and baryonic potential  $\mu$  [17] as follows:

$$U_1^{eff}(\sigma, \pi) = U^{(0)}(\sigma, \pi) - 12 \int \frac{d^3P}{(2\pi)^3} [\sqrt{P^2 + M^2} + T \ln \left( \exp \left( \frac{\mu}{T} - \frac{1}{T} \sqrt{P^2 + M^2} \right) + 1 \right) + T \ln \left( \exp \left( -\frac{\mu}{T} - \frac{1}{T} \sqrt{P^2 + M^2} \right) + 1 \right)]. \quad (1)$$

where, the original mesonic potential at zero temperature and chemical potential is given by

$$U^{(0)}(\sigma, \pi) = \frac{\lambda^2}{4} (\sigma^2 + \pi^2 - \nu^2)^2 + m_\pi^2 f_\pi \sigma. \quad (2)$$

In Eq. (2), the  $\sigma$  and  $\pi$  are the sigma and pion meson fields. The parameters  $\lambda^2$  and  $\nu^2$  are related to the pion and sigma masses, and the pion decay constant  $f_\pi = 93$  MeV

$$\lambda^2 = \frac{m_\sigma^2 - m_\pi^2}{2f_\pi^2}, \quad (3)$$

$$\nu^2 = f_\pi^2 - \frac{m_\pi^2}{\lambda^2}. \quad (4)$$

In Eq. (1), the divergent second term comes from the negative energy states  $\{E = \sqrt{P^2 + M^2}\}$  of the Dirac sea. It can be partly absorbed in the coupling constant  $\lambda^2$  and the constant  $\nu^2$  by using a renormalization procedure [16]. The constituent quark mass is defined as  $M^2 = g^2(\sigma^2 + \pi^2)$ . In Eq. (1), the second term can not be evaluated in closed form as in normally the case for most integrals in statistical mechanics. So we expand the effective potential in the powers of  $M^2$  which ensures that the potential satisfies the chiral symmetry when  $m_\pi \rightarrow 0$ . Thus, the effective potential takes the following form in the one-loop approximation.

$$U_2^{eff}(\sigma, \pi) = U^{(0)}(\sigma, \pi) - \frac{6}{\pi^2} \left( \frac{7\pi^4}{180} T^4 + \frac{\pi^2}{6} T^2 \mu^2 + \frac{1}{12} \mu^4 \right) + 6g^2 \left( \frac{T^2}{12} + \frac{\mu^2}{4\pi^2} \right) (\sigma^2 + \pi^2). \quad (5)$$

In Refs. [23, 24], the authors calculated the critical temperature at zero chemical potential by using one-loop technique in the linear sigma model. They found that two loops or higher-order loops did not affect the critical temperature and the phase transition. They found

that two loops lead to complex terms that are ignored in the calculation of the critical temperature. At finite temperature and chemical potential, the one-loop approximation is successfully predicted the chiral phase transition [25].

Now, we can write the Hamiltonian of quark sigma model at finite temperature and chemical potential including quantized fields as in Refs. [6 → 8]

$$\hat{H}(r) = \frac{1}{2} \{ \hat{P}_\sigma(r)^2 + (\nabla \hat{\sigma}(r))^2 + \hat{P}_\pi(r)^2 + (\nabla \pi(r))^2 \} + U_2^{eff}(\hat{\sigma}, \hat{\pi}) + \hat{\Psi}^\dagger(r) (-i\alpha \nabla) \hat{\Psi}(r) - g(r) \hat{\Psi}^\dagger(r) (\beta \hat{\sigma}(r) + i\beta \gamma_5 \hat{\tau} \cdot \hat{\pi}) \hat{\Psi}(r), \quad (6)$$

where  $\alpha$  and  $\beta$  are the usual Dirac matrices. In the above expression,  $\hat{\Psi}$ ,  $\hat{\sigma}$ , and  $\hat{\pi}$  are quantized field operators with the appropriate static angular momentum expansion [7],

$$\hat{\sigma}(r) = \int_0^\infty \frac{dk k^2}{[2(2\pi)^3 W_\sigma(k)]^{\frac{1}{2}}} [\hat{c}^\dagger(k) e^{-ik \cdot r} + \hat{c}(k) e^{+ik \cdot r}], \quad (7)$$

$$\hat{\pi}(r) = \left[ \frac{2}{\pi} \right]^{\frac{1}{2}} \int_0^\infty dk k^2 \left[ \frac{1}{2W_\pi(k)} \right]^{\frac{1}{2}} \sum_{lmw} j_l(kr) Y_{lm}^*(\Omega_r) [\hat{a}_{lm}^{1w\dagger}(k) + (-)^{m+w} \hat{a}_{l-m}^{1-w}(k)], \quad (8)$$

$$\hat{\Psi}(r) = \sum_{njmw} \left( \langle r | njmw \rangle \hat{d}_{njm}^{\frac{1}{2}w} + \langle r | \bar{n}jmw \rangle \hat{d}_{njm}^{\frac{1}{2}w\dagger} \right), \quad (9)$$

where the  $|njmw\rangle$  and  $|\bar{n}jmw\rangle$  form a complete set of quark and antiquark spinors with angular momentum quantum numbers and spin-isospin quantum numbers  $j, m$ , and  $w$ , respectively. The corresponding conjugate momentum fields have the expansion,

$$\hat{P}_\sigma(r) = i \int_0^\infty dk k^2 \left[ \frac{W_\sigma(k)}{2(2\pi)^3} \right]^{\frac{1}{2}} [\hat{c}^\dagger(k) e^{-\mathbf{k} \cdot \mathbf{r}} - \hat{c}(k) e^{+\mathbf{k} \cdot \mathbf{r}}], \quad (10)$$

$$\hat{P}_\pi(r) = i \left[ \frac{2}{\pi} \right]^{\frac{1}{2}} \int_0^\infty dk k^2 \left[ \frac{W_\pi(k)}{2} \right]^{\frac{1}{2}} \sum_{lmw} j_l(kr) Y_{lm}^*(\Omega_r) [\hat{a}_{lm}^{1w\dagger}(k) - (-)^{m+w} \hat{a}_{l-m}^{1-w}(k)]. \quad (11)$$

Here  $\hat{c}(k)$  destroys a  $\sigma$  with momentum  $\mathbf{k}$  and frequency  $W_\sigma(k) = (k^2 + m_\sigma^2)^{\frac{1}{2}}$  and  $\hat{a}_{lm}^{1w}(k)$  destroys a pion with momentum  $\mathbf{k}$  and corresponding frequency  $W_\pi(k) = (k^2 + m_\pi^2)^{\frac{1}{2}}$  in the isospin-angular momentum state  $\{lm; tw\}$ . For convenience, one constructs the configuration

space pion field functions needed for the subsequent variational treatment by defining the alternative basis operators,

$$\hat{b}_{lm}^{1w} = \int dk k^2 \zeta_l(k) \hat{a}_{lm}^{1w}(k), \quad (12)$$

where  $\hat{a}_{lm}^{1w}(k)$  are basis operators which create a free massive pion with isospin component  $w$  and orbital angular momentum  $(l, m)$ , and  $\zeta_l(k)$  is the variational function. Considering this in configuration space, the pion field function [6] is defined as

$$\Phi_l = \frac{1}{2\pi} \int_0^\infty dk k^2 \frac{\zeta_l(k)}{W_\pi(k)^{\frac{1}{2}}} j_l(r). \quad (13)$$

In the following, only the  $l = 1$  value is used and the angular momentum label will be dropped. The Fock state for the nucleon is taken to be as in Ref. [6]

### III. THE VARIATIONAL PRINCIPLE

In this section, the system of differential equations are presented, following briefly the procedure of Refs. [6, 7 and 8]. The objective of this section is to seek a minimum of the total baryon energy, which is given by

$$E_N = \langle NT_3 J_z | \int_0^\infty d^3r : H(r) : | NT_3 J_z \rangle, \quad (14)$$

The field equations are obtained by minimizing the total energy of the nucleon with respect to the variation of the fields,  $\{u(r), v(r), \sigma(r), \Phi(r)\}$ , as well as the Fock-space parameters,  $\{\alpha, \beta, \gamma\}$ , subjected to the normalization conditions where  $\alpha^2 + \beta^2 + \gamma^2 = 1$ . The total energy of the system is written as

$$E_N = 4\pi \int_0^\infty dr r^2 \varepsilon_N(r). \quad (15)$$

Writing the quark Dirac spinor as

$$\Psi_{\frac{1}{2}m}^{\frac{1}{2}w}(\mathbf{r}) = \begin{pmatrix} u(r) \\ v(r) \sigma \cdot \hat{\mathbf{r}} \end{pmatrix} \chi_{\frac{1}{2}m} \zeta^{\frac{1}{2}w}, \quad (16)$$

the energy density is given by

$$\begin{aligned}
\varepsilon_N(r) = & \frac{1}{2} \left( \frac{d\sigma}{dr} \right)^2 + \frac{\lambda^2}{4} (\sigma^2(r) - \nu^2)^2 - m_\pi^2 f_\pi \sigma(r) + U_0 \\
& - \frac{1}{6\pi^2} \left( \frac{7\pi^4}{180} T^4 + \frac{\pi^2}{6} T^2 \mu^2 + \frac{1}{12} \mu^4 \right) + 6g^2 \left( \frac{T^2}{12} + \frac{\mu^2}{4\pi^2} \right) \sigma^2 \\
& + 3 \left[ u(r) \left( \frac{dv}{dr} + \frac{2}{r} v(r) \right) - v(r) \frac{du}{dr} + g\sigma(r) (u^2(r) - v^2(r)) \right] \\
& + (N_\pi + x) \left( \left( \frac{d\Phi}{dr} \right)^2 + \frac{2}{r^2} \Phi^2(r) \right) + (N_\pi - x) \Phi_p^2(r) - \\
& \alpha \delta g (a + b) u(r) v(r) \Phi(r) + \lambda^2 [x^2 + 2xN_\pi + 81 (\alpha^2 a^2 c^2 + (\beta^2 + \gamma^2) d^2)] \Phi^4(r) + \\
& \lambda^2 (N_\pi + x) (\sigma^2(r) - \nu^2) \Phi^2(r) + 12g^2 \left( \frac{T^2}{12} + \frac{\mu^2}{4\pi^2} \right) (N_\pi + x) \Phi(r)^2
\end{aligned} \tag{17}$$

where  $N_\pi$  is the average pion number

$$N_\pi = 9 (\alpha^2 a^2 + (\beta^2 + \gamma^2) c^2), \tag{18}$$

and  $\delta$  takes the following values for the nucleon quantum numbers:

$$\delta_N = (5\beta + 4\sqrt{2}\gamma) / \sqrt{3}. \tag{19}$$

The function  $\Phi_p(r)$  is obtained from  $\Phi(r)$  by double folding:

$$\Phi_p(r) = \int_0^\infty w(r, r') \Phi(\mathbf{r}) r^2 dr', \tag{20}$$

$$w(r, r') = \frac{2}{\pi} \int_0^\infty dk k^2 w(k) j_1(kr) j_1(kr'). \tag{21}$$

For fixed  $\alpha, \beta$ , and  $\gamma$ , the stationary functional variations are expressed by

$$\delta \left[ \int_0^\infty dr r^2 (\varepsilon_N(r) - 3\epsilon (u^2(r) + v^2(r)) - 2k\Phi\Phi_p(r)) \right] = 0, \tag{22}$$

where the parameter  $k$  enforces the pion normalization condition,

$$8\pi \int_0^\infty \Phi(r) \Phi_p(r) r^2 dr = 1, \tag{23}$$

and  $\epsilon$  fixes the quark normalization,

$$4\pi \int_0^\infty (u^2(r) + v^2(r)) r^2 dr = 1. \tag{24}$$

Minimizing the Hamiltonian yields the four nonlinear coupled differential equations,

$$\frac{du}{dr} = -2(g\sigma + \epsilon)v(r) - \frac{1}{3}\alpha\delta(a+b)g\Phi(r)u(r), \quad (25)$$

$$\frac{dv}{dr} = -\frac{2}{r}v(r) - 2(g\sigma(r) - \epsilon)u(r) + \frac{1}{3}\alpha\delta(a+b)g\Phi(r)u(r), \quad (26)$$

$$\begin{aligned} \frac{d^2\sigma}{dr^2} = & -\frac{2}{r}\frac{d\sigma}{dr} - m_\pi^2 f_\pi + 3g(u^2(r) - v^2(r)) + 2\lambda^2(N_\pi + x)\Phi^2(r)\sigma(r) + \\ & + \lambda^2(\sigma^2(r) - \nu^2)\sigma(r) + 12g^2\left(\frac{T^2}{12} + \frac{\mu^2}{4\pi^2}\right)\sigma(r) \end{aligned} \quad (27)$$

$$\begin{aligned} \frac{d^2\Phi}{dr^2} = & -\frac{2}{r}\frac{d\Phi}{dr} + \frac{2}{r^2}\Phi(r) + \frac{1}{2}\left(1 - \frac{x}{N_\pi}\right)m_\pi^2\Phi + \frac{\lambda^2}{2}\left(1 + \frac{x}{N_\pi}\right)(\sigma^2(r) - \nu^2)\Phi(r) - \\ & \frac{\alpha}{N_\pi}(a+b)g\delta u(r)v(r) + \frac{\lambda^2}{N_\pi}[x^2 + 2xN_\pi + 81(\alpha^2 a^2 c^2 + (\beta^2 + \gamma^2)d^2)]\Phi^3(r) \\ & - \frac{k}{N_\pi}\Phi_p(r) + 24g^2\left(\frac{T^2}{12} + \frac{\mu^2}{4\pi^2}\right)\Phi(r)\left(1 + \frac{x}{N_\pi}\right), \end{aligned} \quad (28)$$

with the eigenvalues  $\epsilon$  and  $k$ . The above equations consist of two quark equations for  $u$  and  $v$  where  $\sigma(r)$  and  $\Phi(r)$  appear as potentials and two Klein-Gordon equations with  $u(r)v(r)$  and  $(u^2(r) - v^2(r))$  are source terms. The coefficients  $a$ ,  $b$ , and  $c$  are functions in the coherence parameter  $x$  and the field equations are solved for the fixed coherence parameter  $x$  and the fixed Fock-space parameters  $(\alpha, \beta, \gamma)$  as in Refs. [6,13].

#### IV. THE NUCLEON PROPERTIES

The expectation value of the energy is minimized with respect to  $(\alpha, \beta, \gamma)$  by diagonalizing the energy matrix

$$\begin{bmatrix} H_{\alpha\alpha} & H_{\alpha\beta} & H_{\alpha\gamma} \\ H_{\alpha\beta} & H_{\beta\beta} & H_{\beta\gamma} \\ H_{\alpha\gamma} & H_{\beta\gamma} & H_{\gamma\gamma} \end{bmatrix} \begin{bmatrix} \alpha \\ \beta \\ \gamma \end{bmatrix} = E \begin{bmatrix} \alpha \\ \beta \\ \gamma \end{bmatrix}, \quad (29)$$

where each  $H$  entry of the matrix is related to a corresponding density as follows:

$$H_{\alpha\beta} = 4\pi \int r^2 E_{\alpha\beta}(r) dr, \quad (30)$$

with similar definitions for the other entries. The functions for a nucleon are

$$\begin{aligned} E_{\alpha\alpha} = & E_0(r) + 18a^2\Phi_p^2 + 9a^2\lambda^2(2x + 9c^2)\Phi^4(r) + 9\lambda^2a^2(\sigma^2(r) - \nu^2)\Phi^2(r) + \\ & 108a^2\Phi^2(r)g^2\left(\frac{T^2}{12} + \frac{\mu^2}{4\pi^2}\right), \end{aligned} \quad (31)$$



$$E_{\beta\beta} = E_0(r) + 18c^2\Phi_P^2 + 9\lambda^2(2xc^2 + 9d^2)\Phi^4(r) + 9\lambda^2c^2(\sigma^2(r) - \nu^2)\Phi^2(r) + 108c^2\Phi^2(r)g^2\left(\frac{T^2}{12} + \frac{\mu^2}{4\pi^2}\right), \quad (32)$$

$$E_{\gamma\gamma} = E_0(r) + 18c^2\Phi_P^2 + 9\lambda^2(2xc^2 + 9d^2)\Phi^4(r) + 9\lambda^2c^2(\sigma^2(r) - \nu^2)\Phi^2(r) + 108c^2\Phi^2(r)g^2\left(\frac{T^2}{12} + \frac{\mu^2}{4\pi^2}\right), \quad (33)$$

$$E_{\alpha\beta} = -2g(a+b)\Phi(r)u(r)v(r)\frac{2\sqrt{2}}{\sqrt{3}}, \quad (34)$$

$$E_{\alpha\gamma} = -2g(a+b)\Phi(r)u(r)v(r)\frac{5}{\sqrt{3}}, \quad (35)$$

where:

$$\begin{aligned} E_0(r) = & \frac{1}{2} \left( \frac{d\sigma}{dr} \right)^2 + \lambda^2 x^2 \Phi^4(r) + 3g\sigma(r)(u^2(r) - v^2(r)) - m_\pi^2 f_\pi \sigma(r) \\ & + 3[u(r)\left(\frac{dv}{dr} + \frac{2}{r}v(r) - v(r)\right)\frac{du}{dr}] + \frac{\lambda^2}{4}(\sigma^2(r) - \nu^2)^2 + \lambda^2 x(\sigma^2(r) - v^2)\Phi^2(r) \\ & + 6g^2\left(\frac{T^2}{12} + \frac{\mu^2}{4\pi^2}\right)\sigma^2 + U_0, \end{aligned} \quad (36)$$

where  $U_0$  is the minimum of potential  $U$ .

### A. Mass of the Nucleon

In this subsection, we calculate the total energy of the nucleon, which consists of quark, sigma, pion, quark-sigma interaction, quark-pion interaction, and meson static energy contributions. The nucleon mass was derived as in Ref. [8]:

$$(K.E)_{quark} = \int_0^\infty (g\sigma\rho_s(r) + \epsilon\rho_w(r) + g\pi\rho_p(r))r^2 dr, \quad (37)$$

where  $\rho_s$ ,  $\rho_p$ , and  $\rho_w$  are the quark scalar density, pseudoscalar density, and vector density, respectively. Similarly, one can find the meson kinetic contribution:

$$\begin{aligned} (K.E)_{sigma} = & \frac{1}{2} \int_0^\infty \sigma(r)(-m_\pi^2 f_\pi + 3g(u^2(r) - v^2(r)) + \lambda^2(N_\pi + x)\Phi^2(r)\sigma(r) + \\ & + \lambda^2(\sigma^2(r) - \nu^2)\sigma(r) + 12g^2\left(\frac{T^2}{12} + \frac{\mu^2}{4\pi^2}\right)\sigma)r^2 dr \end{aligned} \quad (38)$$

$$\begin{aligned} (K.E)_{pion} = & \frac{1}{2} \int_0^\infty \Phi(r)\left(\frac{2}{r^2}\Phi(r) + \frac{1}{2}\left(1 - \frac{x}{N_\pi}\right)m_\pi^2\Phi + \frac{\lambda^2}{2}\left(1 + \frac{x}{N_\pi}\right)(\sigma^2(r) - v^2)\Phi(r) - \right. \\ & \frac{\alpha}{4N_\pi}(a+b)g\delta u(r)v(r) + \frac{\lambda^2}{N_\pi}[x^2 + 2xN_\pi + 81(\alpha^2 a^2 c^2 + (\beta^2 + \gamma^2)d^2)]\Phi^3(r) \\ & \left. - \frac{k}{N_\pi}\Phi_p(r) + 24g^2\left(\frac{T^2}{12} + \frac{\mu^2}{4\pi^2}\right)\Phi(r)\left(1 + \frac{x}{N_\pi}\right)\right)r^2 dr. \end{aligned} \quad (39)$$

The quark-meson interaction energy takes the form

$$E_{q-sigma} = - \int_0^\infty g\sigma\rho_s(r)r^2dr \quad (40)$$

$$E_{q-pion} = - \int_0^\infty g\sigma\rho_p(r)r^2dr, \quad (41)$$

and the meson-meson interaction energy is

$$E_{meson-meson} = \int_0^\infty \left( \frac{\lambda^2}{4} (\hat{\sigma}^2 + \hat{\pi}^2 - \nu^2)^2 - f_\pi m_\pi^2 \hat{\sigma} - \frac{6}{\pi^2} \left( \frac{7\pi^4}{180} T^4 + \frac{\pi^2}{6} T^2 \mu^2 + \frac{1}{12} \mu^4 \right) + 6g^2 \left( \frac{T^2}{12} + \frac{\mu^2}{4\pi^2} \right) (\sigma^2 + \pi^2) \right) r^2 dr. \quad (42)$$

## V. RESULTS AND DISCUSSION

In this section, we examine our calculations obtained from solving the system of differential equations (25  $\rightarrow$  28). To solve the system, we apply the modified COLSYS code at finite temperature and chemical potential. The code is used before in many works such as in Refs. [6  $\rightarrow$  8]. The initial parameters at zero temperature and chemical potential are used as initial parameters at finite temperature and chemical potential, where the mass of the sigma particle in the data group ranges from 400 to 1200 MeV [26] and the coupling constant  $g = 3.5 \rightarrow 6$  are used as free parameters. Other parameters such as  $m_\pi$  and  $f_\pi$  are fixed from experimental data. The iteration procedure is implemented as follows. For fixed values of  $x$ ,  $\alpha$ ,  $\beta$ , and  $\gamma$ , the differential equations with the corresponding boundary conditions are solved until self-consistency is achieved.

The task of this section is to show the effect finite temperature and chemical potential on nucleon properties. So, we divide the discussion into two parts:

In the first part, the effect of finite chemical potential on the nucleon properties is discussed as follows: In Fig. (1), we displayed the effect of finite chemical potential on the sigma, the pion, and the quark fields at zero temperature and chemical potential in comparison with their behavior at zero temperature and finite chemical potential. In Fig. (1), we have plotted the above fields as functions of the distance  $r$ . We note that the sigma field increases with increasing distance  $r$ , in which the sigma field takes a maximum value when  $r \rightarrow \infty$ . The function  $u(r)$  has maximum value at  $r = 0$  and then it decreases until it reaches zero as  $r \rightarrow \infty$ . The function  $v(r)$  has similar behavior as the pion field. By increasing chemical potential up to 100 MeV, we note that the qualitative features of the

sigma and pion fields are similar in the two cases where the fields shift to lower values in comparison with the zero-temperature and chemical potential case. Hence, the meson field is sensitive to the change of the chemical potential in comparison with their behavior at zero temperature and chemical potential. Therefore, the change in the mesonic contributions will be affected in the observables of the nucleon as it will be explained next.

Now, we examine the change in the dynamic of the nucleon energy at finite chemical potential. In Figs. (2, 3 and 4), we have plotted the kinetic energy density of the quark, sigma and the pion fields and the interaction between them at finite chemical potential and zero temperature in comparison with their values at  $(T = 0, \mu = 0)$ . In Fig. 2, the kinetic energies density of quark, sigma and pion fields are plotted as functions of  $r$  at finite chemical potential and zero-temperature in comparison with their behavior at  $(T = 0, \mu = 0)$ . We note that the quark and sigma kinetic energy density decreases with increasing  $r$  up to 1 fm and has a fixed value when  $r$  tends to infinity. The pion kinetic energy density increases up to 0.5 fm and then it decreases with increasing distance  $r$  up to 1 fm and then it has a fixed value as  $r \rightarrow \infty$ . By increasing chemical potential up to 100 MeV, we note that the kinetic energy density for each field is shifted to lower values, in particular, in the range  $r = 0 \rightarrow 1$  fm. Thus, we deduce that the mesonic contributions in these quantities are sensitive only at lower values of the distance  $r$ .

In Fig. 3, the quark-meson density interaction is plotted as a function of  $r$ . We note that the quark-sigma density interaction increases with increasing  $r$  up to 1 fm and then it has a fixed value when  $r$  increases. The quark-pion density has the smallest values in comparison with the quark-sigma density, thus it appears as a fixed function. By increasing chemical potential, we note that each field shifts to higher values at smaller values of  $r$ . A similar situation takes place with respect to the meson-meson density interaction that decreases with increasing distance  $r$ . By increasing chemical potential, the curve is shifted to higher-values at all values of  $r$ . The effect of the chemical potential clearly appears when  $r$  increases. Therefore, the meson-meson density interaction plays an essential role at all values of  $r$ . Thus, this effect will act on the mesonic contributions of the nucleon energy. The coherence parameter  $x$  plays an important role in the present work. The nucleon mass is plotted as a function of  $x$  at  $T = 0, \mu = 270$  MeV as in Fig. 5. We note that an increase in the coherence parameter  $x$  leads to an increase in the nucleon mass due to the fact that the coherence parameter  $x$  increases the pionic contributions in the present model.

TABLE I: The energy calculations of nucleon mass for value of coherence parameter  $x = 1$  at  $m_\pi = 139.6$  MeV,  $m_\sigma = 472$  MeV and  $g = 4.5$ . All observables in MeV.

Quantity	$T = 0$ and $\mu = 0$	$T = 0$ and $\mu = 270$ MeV
Kinetic energy of quark	463.390	312.538
Kinetic energy of sigma	249.200	0.530
Kinetic energy of pion	174.794	93.232
Quark-sigma interaction	92.840	-0.671
Quark-pion interaction	$-1 \times 10^{-4}$	0.745
Pion-sigma interaction	136.47	1012
Nucleon Mass	1069.835	1418.86

In Table V, we calculate constituents of the nucleon energy at zero temperature and chemical potential in comparison with the nucleon energy at finite chemical potential. We note that the kinetic energy of the sigma, pion and quark fields decrease with increasing chemical potential, while the meson-meson interaction energy strongly increases. Therefore, we find that the nucleon mass increases with increasing chemical potential. In addition, by increasing chemical potential above 270 MeV, we find that the nucleon mass decreases.

Here, we investigate other nucleon properties such as, the mean-square radius of proton  $\langle r^2 \rangle_p$  and neutron  $\langle r^2 \rangle_n$ , the magnetic moment of proton  $\mu_p$  and neutron  $\mu_n$ , the coupling constant  $\frac{g_A}{g_v}$ , and the pion-nucleon coupling constant  $g_{\pi NN}^G$ . In Table V, we display the change in the mesonic and quark contributions in these quantities when the chemical potential is taken equal to 270 MeV. We note that the quark contributions in  $\langle r^2 \rangle_p$  strongly increases with increasing chemical potential, while the mesonic contributions decreases with increasing chemical potential. The total effect of quark and mesonic contributions lead to an increase of  $\langle r^2 \rangle_p$  by increasing chemical potential. A similar situation takes place with respect to  $\langle r^2 \rangle_n$ . In the magnetic moment of proton, we note that the mesonic and quark contributions decrease with increasing chemical potential. Therefore, the magnetic moment of the proton decreases at finite chemical potential in comparison with its value at zero temperature and

TABLE II: The observables of the nucleon calculated for a value of the coherence parameter  $x = 1$  at  $m_\pi = 139.6$  MeV,  $m_\sigma = 472$  MeV and  $g = 4.5$ .

	$T = 0$ and $\mu = 0$			$T = 0$ and $\mu = 270$ MeV		
Quantity	Quark	Meson	Total	Quark	Meson	Total
$\langle r^2 \rangle_p$	$7.217 \times 10^{-1}$	$2.8605 \times 10^{-2}$	0.750	2.535	$-2.584 \times 10^{-5}$	2.535
$\langle r^2 \rangle_n$	$2.232 \times 10^{-2}$	$-2.8605 \times 10^{-2}$	$-6.277 \times 10^{-3}$	$-9.187 \times 10^{-6}$	$2.584 \times 10^{-5}$	$1.665 \times 10^{-5}$
$\mu_p$	1.734	0.175	1.909	0.750	$6.659 \times 10^{-7}$	0.750
$\mu_n$	-1.262	-0.175	-1.437	0.500	$6.659 \times 10^{-7}$	-0.500
$\frac{g_A}{g_v}$	1.1624	0.371	1.534	0.296	$2.614 \times 10^{-7}$	0.296
$g_{\pi NN}^G$	0.873	0.278	1.151	0.417	$1.90 \times 10^{-7}$	0.417

chemical potential. A similar situation takes place with respect to the magnetic moment of neutron. The coupling constant  $\frac{g_A}{g_v}$  and the pion-nucleon constant  $g_{\pi NN}^G$  play an essential role in the present model. We note that two quantities decrease with increasing chemical potential.

Next, in the second part, we study the effect of finite temperature at zero chemical potential in comparison with corresponding values at zero temperature and chemical potential. We discuss the effect of finite temperature on the dynamic of the fields. In Fig. 6, the sigma, the pion and the components of the quark fields are plotted as functions of  $r$  at finite temperature in comparison with the behavior at zero temperature and chemical potential. The sigma field increases with increasing distance  $r$ , in which the sigma field has a maximum value as  $r \rightarrow \infty$ . Also, the pion field takes the form of the P-wave function that increases up to 0.5 fm and it decreases with increasing distance  $r$ . The components of the quark fields  $u(r)$  and  $v(r)$  have maximum values at  $r = 0$  and tends to zero at infinity. The  $v(r)$  component of the quark field takes a similar behavior to the pion field. By increasing temperature, we note that all fields are shifted to lower values. Therefore, the change in the thermal state leads to a change in the mesonic and quark contributions which will have an effect on the dynamics of the fields.

In Fig. 7, the kinetic energy of the quark, sigma, and pion are plotted as functions of  $r$  at zero and finite temperature at vanishing chemical potential. We note that the quark energy density decreases with increasing  $r$  up to 1 fm and then takes fixed values when  $r \rightarrow \infty$ . A similar situation takes places with respect to the sigma kinetic energy density, the difference between them appears at smallest values of  $r$ . The kinetic energy density of the pion takes the form of P-wave function. By increasing temperature, we find that the kinetic energy density of the quark, the sigma and the pion fields are shifted to lower values. In Fig. 8, the quark-meson density interaction is plotted. We note that the quark-sigma density interaction increases with increasing distance  $r$  up 1.2 fm and then it has a fixed value when the distance  $r$  increases. The quark-pion density interaction has smallest values in comparison with its behavior at finite temperature. By increasing temperature, we note the quark-meson density interaction shifts to higher-values at smaller values of  $r$ . In Fig. 9, the meson-meson density decreases with increasing  $r$ . By increasing temperature, we note that the curve shifts to higher values when  $r$  increases. Therefore. the meson-meson density plays an essential role for increasing nucleon energy due to an increase in the mesonic contributions at larger values of the distance  $r$ .

In Table V, we display the kinetic energy of the quark, the sigma and the pion, the quark-meson interaction, and the meson-meson interaction at  $T = 100$  MeV and  $\mu = 0$  in comparison with their values at zero temperature and chemical potential.

We note that the pion-sigma interaction increases strongly in comparison with its value at  $T = 0$ ,  $\mu = 0$ . Since, the meson-meson interaction is sensitive to the changes at any value of the distance  $r$ . The kinetic energy of quark, sigma, and pion decrease with increasing temperature. The strong change of the mesonic potential leads to an increase in the nucleon mass up to  $T = 100$  MeV. This result is in agreement with the results of Ref. [21], in which the soliton energy increases with increasing temperature at zero density using the Nambu-Jona- Lasinio model.

Next, we examine other nucleon properties given in Table V: the mean-square radius of proton  $\langle r^2 \rangle_p$  and neutron  $\langle r^2 \rangle_n$ , the magnetic moment of proton  $\mu_p$  and neutron  $\mu_n$ , the

TABLE III: The energy calculations of nucleon mass for value of coherence parameter  $x = 1$  at  $m_\pi = 139.6$  MeV,  $m_\sigma = 472$  MeV and  $g = 4.5$ . All observables in MeV.

Quantity	$T = 0$ and $\mu = 0$	$T = 100$ MeV and $\mu = 0$
Kinetic energy of quark	463.390	210
Kinetic energy of sigma	249.200	-0.172
Kinetic energy of pion	174.794	96.768
Quark-sigma interaction	92.840	32.408
Quark-pion interaction	$-1 \times 10^{-4}$	-0.003
Pion-sigma interaction	136.47	1959.043
Nucleon Mass	1069.835	2298.222

TABLE IV: The observables of the nucleon calculated for coherence parameter  $x = 1$  at  $m_\pi = 139.6$  MeV,  $m_\sigma = 472$  MeV and  $g = 4.5$ .

	$T = 0$ and $\mu = 0$			$T = 100$ MeV and $\mu = 0$		
Quantity	Quark	Meson	Total	Quark	Meson	Total
$\langle r^2 \rangle_p$	$7.217 \times 10^{-1}$	$2.8605 \times 10^{-2}$	0.750	2.974	$-3.042 \times 10^{-5}$	2.974
$\langle r^2 \rangle_n$	$2.232 \times 10^{-2}$	$-2.8605 \times 10^{-2}$	$-6.277 \times 10^{-3}$	$-1.089 \times 10^{-5}$	$3.0429 \times 10^{-5}$	$1.954 \times 10^{-5}$
$\mu_p$	1.734	0.175	1.909	2.939	$7.462 \times 10^{-7}$	2.939
$\mu_n$	-1.262	-0.175	-1.437	-1.959	$7.462 \times 10^{-7}$	-1.959
$\frac{g_A}{g_v}$	1.1624	0.371	1.534	$5.046 \times 10^{-1}$	$3.76 \times 10^{-8}$	0.5046
$g_{\pi NN}^G$	0.873	0.278	1.151	$3.711 \times 10^{-1}$	$7.57 \times 10^{-8}$	0.3787

coupling constant  $\frac{g_A}{g_v}$ , and the pion-nucleon coupling constant  $g_{\pi NN}^G$ . We note that the  $\langle r^2 \rangle_p$  increases with increasing temperature, where the mesonic contributions decrease in comparison with its value at  $T = 0$  and  $\mu = 0$ , while the quark contributions increase three times in comparison with its value at  $T = 0$  and  $\mu = 0$ . Thus the quark contributions have more effect on the value of the mean-square radius of proton. Therefore, we note that  $\langle r^2 \rangle_p$  increases with increasing temperature. A similar situation takes place with respect to  $\langle r^2 \rangle_n$ .

An increase in  $\langle r^2 \rangle_p$  is noted in Refs. [12, 13, 14] with increasing temperature, in which the quark sigma model is applied in the mean-field approximation. The magnetic moment of the proton and neutron increase with increasing temperature. We note that the quark contributions strongly increase with increasing temperature, while the mesonic contributions decrease with increasing temperature. The coupling constant  $\frac{g_A}{g_v}$  and the pion-nucleon coupling constant  $g_{\pi NN}^G$  are also calculated. We note that the quark and mesonic contributions decrease with increasing temperature. Therefore, we find that  $\frac{g_A}{g_v}$  and  $g_{\pi NN}^G$  decrease with increasing temperature. In the present work, we find that the nucleon mass and mean-square radius of the proton increase with increasing temperature, while the pion-nucleon coupling constant decreases with increasing temperature. This indicates that a deconfinement phase is satisfied at higher values of the temperature and in agreement with QCD finite energy sum rule [13].

## VI. SUMMARY AND CONCLUSIONS

In the previous section, we gave qualitative and quantitative description of the meson fields and the nucleon properties at finite temperature and chemical potential. So, we need to show clearly the novelty in this work. We gave in the section of introduction that most of nucleon properties at finite temperature and chemical potential are carried out in the framework of chiral sigma model and NJL model in the mean-field approximation. The coherent-pair approximation (CPA) is applied in the chiral quark model at finite temperature only in the previous work [14]. CPA is a powerful nonperturbative method to go beyond the mean-field approximation by fully taking thermal and quantum fluctuations into account [14]. In addition, one avoids assumptions like the hedgehog structure of the quark and pion fields that are taken in many works at finite temperature and density such as in Ref. [17] and the references therein. So far no attempt has been made to include the finite chemical potential by using the coherent-pair approximation.

The qualitative features of sigma and pion fields are in agreement with mean-field approximation results at finite temperature and chemical potential. In addition, the sigma and pion fields are sensitive to change of the temperature and chemical potential. The pion-nucleon coupling constant and pion decay constant decreases with increasing temperature and chemical potential, which indicates that a deconfinement phase transition is satisfied in



the present work at higher values of the temperature. The mean-square radius of proton  $\langle r^2 \rangle_p$  and neutron  $\langle r^2 \rangle_n$ , the magnetic moment of proton  $\mu_p$  and neutron  $\mu_n$  are investigated at finite chemical potential. The qualitative agreement of present results are discussed in comparison with other works. The effect of coherence of the parameter  $x$  on the nucleon mass is studied.

In the coherent-pair approximation, we conclude that the nucleon properties are strong changed by including finite chemical potential. The coherence parameter  $x$  plays an important for changing the nucleon mass at finite chemical potential, since an increase in  $x$  leads to increasing in the pionic contributions in the energy of nucleon at finite chemical potential.

We hope to extend this work to include external magnetic field which will give better understanding into the complex vacuum structure of quantum chromodynamic (QCD) theory which describes relevant features of particle physics in the early universe and the neutron stars.

- 
- [1] M. Gyulassy and L. McLerran, Nul. Phys. **A 750**, 30 (2005).
  - [2] J. I. Kapusta, J. Phys. **G 34** S295 (2007).
  - [3] T. Inagaki, D. Kimura, H. Kohyama, and A. Kvinikhidze, Phys. Rev. D **85**, 076002 (2012).
  - [4] Y. Nambu and G. Jona-Lasinio, Phys. Rev. **122**, 345 (1961).
  - [5] M. Birse and M. Banerjee, Phys. Rev. D **31**, 118 (1985).
  - [6] K. Goeke, M. Harve, F. Gru, and J. N. Urbano, Phys. Rev. D **37**, 754 (1988).
  - [7] T.S.T. Aly, J. A. McNeil, and S. Pruess, Phys. Rev. D **60**, 1114022 (1999).
  - [8] M. Abu-Shady and M. Rashdan, Phys. Rev. C **81**, 015203 (2010).
  - [9] M. Abu-Shady, Mod. Phys. Lett. A **24**, 1617, (2009).
  - [10] M. Rashdan, M. Abu-Shady, and T.S.T Ali, Inter. J. Mod. Phys. A **22**, 2673 (2007).
  - [11] W. Broniowski and B. Golli, Nucl. Phys. A **714**, 575 (2003).
  - [12] C. V. Christov, E. R. Arriola, and K. Goeke, Nul. Phys. A **556**, 641 (1993).
  - [13] C. A. Dominguez, C. Van Gend and M. Loewe, Nucl. Phys. B Proc. Supp. **86**, 413 (2000).
  - [14] M. Abu-Shady and H. M. Mansour, Phys. Rev. C **85**, 055204 (2012).
  - [15] N. Bilic and Nikolic, Eur. Phys. J. C **6**, 515 (1999).
  - [16] O. Scanvenius, A. Moscsy, I. N. Mishustin, and D. H. Rischke, Phys. Rev. C **64**, 045202

- (2001).
- [17] H. Mao, T.-Z. Wei and J.-S. Jin, Phys. Rev. C **88**, 035201 (2013).
  - [18] T. H. Phat and N. V. Thu, Eur. Phys. J. C **71**, 1810 (2011).
  - [19] B. J. Schaefer, J. M. Pawłowski, and J. Wambach. Phys. Rev. D **76**, 074023 (2007).
  - [20] H. Mao, Minji Yao, and Wei-Qin Zhao, Phys. Rev. C **77**, 055205 (2008).
  - [21] J. Berger and C. V. Christov, Nucl. Phys. A **609**, 537 (1996).
  - [22] Cheng-fu Mu, Yin Jiang, Peng-fei Zhuang, and Yu-xin, Phys. Rev. D **85**, 014033 (2012).
  - [23] L. Dolan and R. Jackiw, Phys. Rev. D **9**, 3320 (1974).
  - [24] A. Das, "finite temperature field theory", Chap. **6**, World Scientific publishing Co. Pte. Ltd (1997) and references therein.
  - [25] M. Abu-Shady, Mod. Phys. Lett. A **29**, 1450176 (2014).
  - [26] D. I. Diakonov, V. Yu. Petrov, and M. Praszalowicz, Phys. B**323**, 53 (1989)

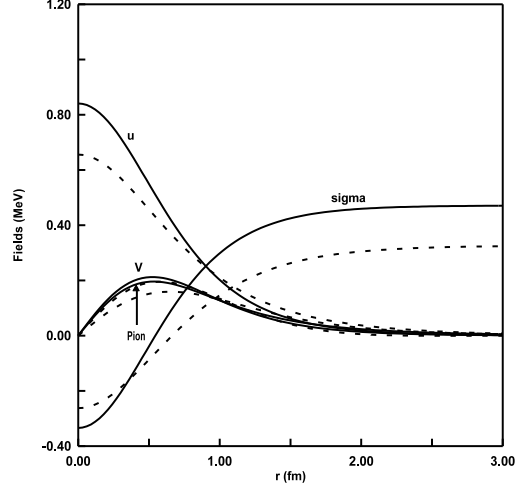


FIG. 1: Sigma, pion, and the components  $(u(r), v(r))$  of the quark fields are plotted as functions of the radial distance  $r$ , where the continuous curves are for  $T = 0$  and  $\mu = 0$  and the dashed curves are for  $T = 0$  and  $\mu = 100$  MeV.

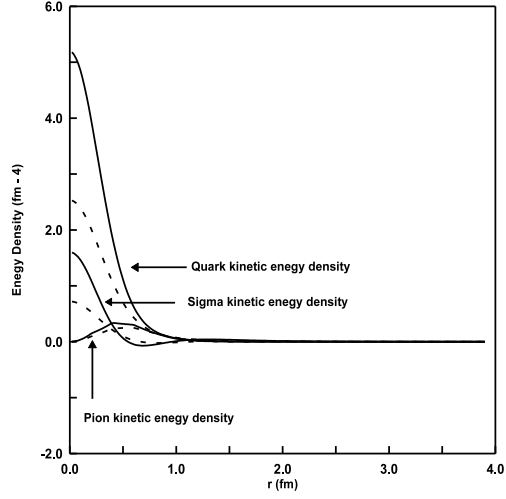


FIG. 2: The kinetic energy density of the quark, sigma, and the pion are plotted as a function of  $r$ , where the continuous curves are for  $T = 0$  and  $\mu = 0$  and the dashed curves are for  $T = 0$  and  $\mu = 100$  MeV.

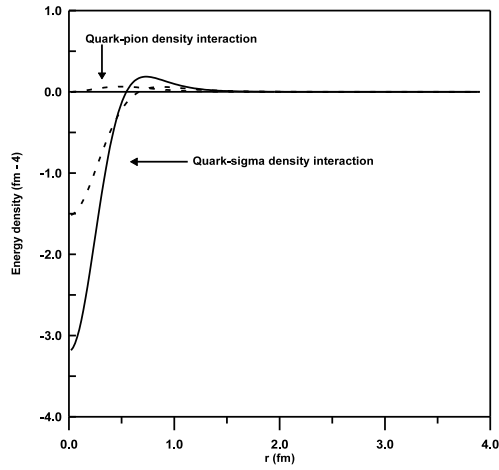


FIG. 3: The quark-meson density interaction is plotted as a function of  $r$ , where the continuous curves are for  $T = 0$  and  $\mu = 0$  and the dashed curves are for  $T = 0$  and  $\mu = 100$  MeV.

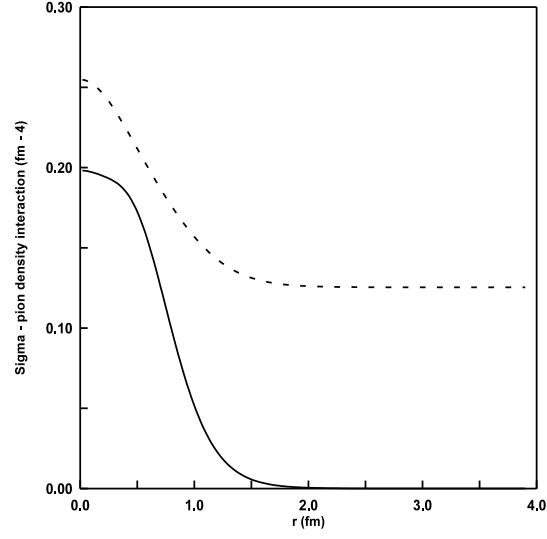


FIG. 4: Meson-meson density interaction is plotted as a function of  $r$ , where the continuous curves are for  $T = 0$  and  $\mu = 0$  and the dashed curves are for  $T = 0$  and  $\mu = 100$  MeV.

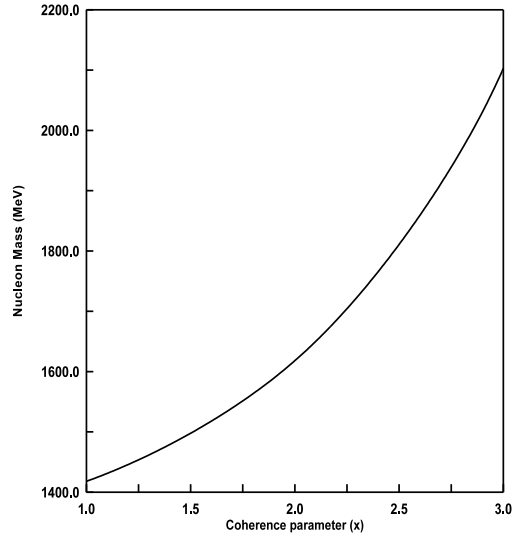


FIG. 5: Nucleon mass is plotted as a function of the coherence parameter  $x$  at for  $T = 0$  and  $\mu = 270$  MeV.

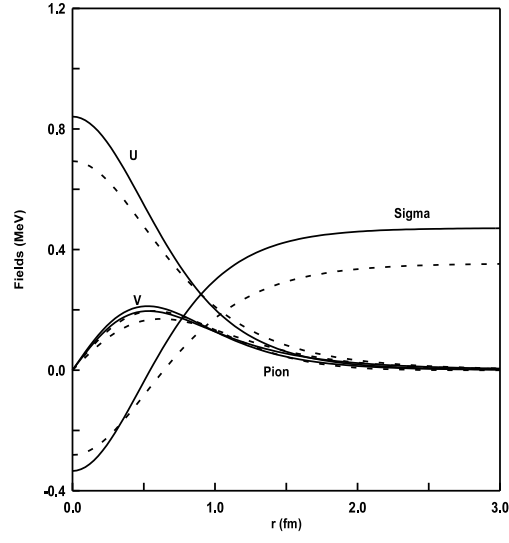


FIG. 6: Sigma, pion, and the components  $(u(r), v(r))$  of the quark fields are plotted as functions of  $r$ , where the continuous curves are for  $T = 0$  and  $\mu = 0$  and the dashed curves are for  $T = 50$  MeV and  $\mu = 0$ .

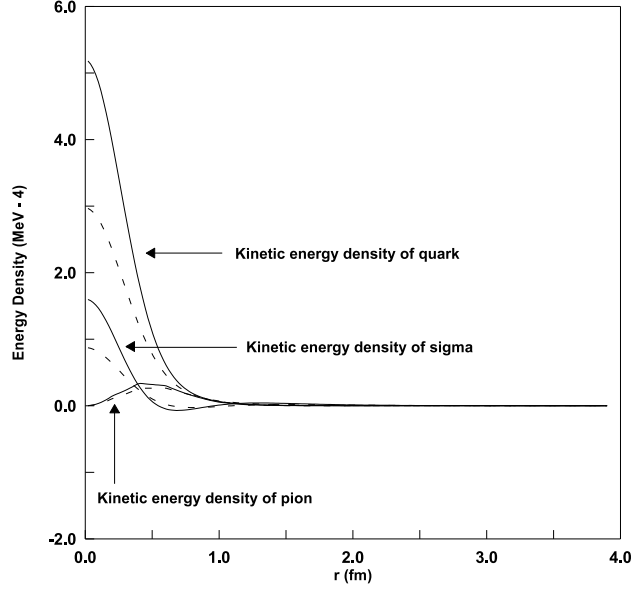


FIG. 7: The kinetic density of field is plotted as a function of  $r$ , where the continuous curves are for  $T = 0$  and  $\mu = 0$  and the dashed curves are for  $T = 50$  MeV and  $\mu = 0$ .

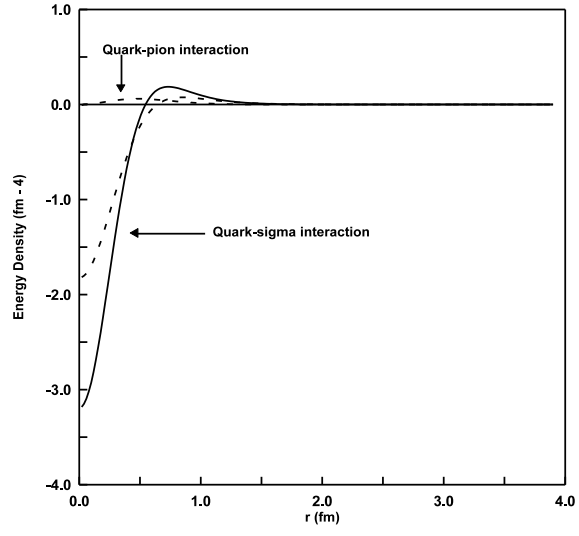


FIG. 8: The quark-meson density interaction is plotted as a function of  $r$ , where the continuous curves are for  $T = 0$  and  $\mu = 0$  and the dashed curves are for  $T = 50$  MeV and  $\mu = 0$ .



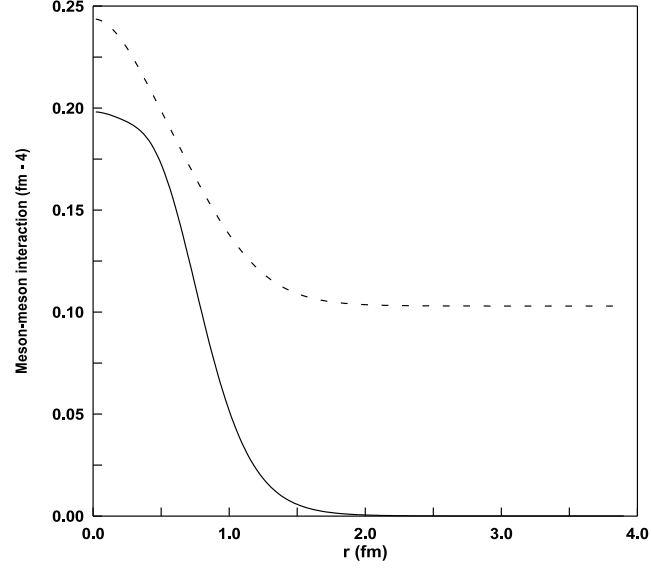


FIG. 9: The meson-meson density interaction is plotted as a function of distance  $r$ , where the continuous curves are for  $T = 0$  and  $\mu = 0$  and the dashed curves are for  $T = 50$  MeV and  $\mu = 0$ .